Innovative passive yaw damper to increase the stability and curve-taking performance of high-speed railway vehicles

Gioele Isacchi[1], Francesco Ripamonti[1], Matteo Corsi[2]

[1] *Politecnico di Milano, Piazza Leonardo da Vinci, 32*
20133 Milano, Italy, gioele.isacchi@polimi.it

[2] *KONI BV, Korteweg 2, 3261 NH Oud-Beijerland,*
Netherlands, matteo.corsi@itt.com

Abstract

Yaw dampers are implemented on high-speed trains to reduce their tendency towards unstable movement (hunting) while running at high-speed. Although they have a positive influence on the vehicle's stability, these devices impose a steering resistance action on the bogies while negotiating tight curves at low speed, and so standard passive devices must be designed taking conflicting objective functions into account. This paper presents an innovative yaw damper able to overcome this trade-off by introducing a passive solution able to modify this component's working behaviour during different vehicle operating conditions. To quantify the efficacy of this solution, numerical models of innovative and standard dampers were developed and validated by means of experimental tests. Then, they were co-simulated with a multibody model of a real test case vehicle running under different operating conditions.

Keywords: Railway dynamics, yaw damper, multibody dynamics, curve-taking performance, vehicle stability.

1 Introduction

The growth in the number of high-speed railway lines and the increase in their overall length around the world is a consolidated trend. This transport system is increasing its competitiveness, thanks to its capability of reducing the ecological impact [1] and its high safety standards. From the passenger's point of view, when it comes to high-speed railway vehicles, the shorter the travel time the higher the

appeal [2]**.** For this reason, one of the most effective methods used to increase the competitiveness of these vehicles is to enhance their speed without reducing their safety level.

In recent years, the continuous increase in the commercial speed of railway vehicles has been supported by the development of innovative suspension components able to guarantee higher safety standards, superior comfort levels and reduced travel times. A lot of different devices, characterised by semi-active or active layouts and by various control logics, have been studied and implemented in recent years, in the various suspension components of railway vehicles [3]**.**

In relation to the secondary suspension stage, one of the components that has the greatest influencing on the vehicle's stability is the yaw damper. Thanks to its dissipating action, this device suppresses the tendency of railway vehicles to exhibit hunting (an unstable motion) when running at high-speed [4]. According to [5], it can be stated that the higher the equivalent damping of the yaw dampers, the higher the critical speed of the vehicle. On the other hand, the presence of stiff yaw dampers reduces the vehicle's curve-taking performance when taking tight curves at low-speed, by increasing the steering resistance of the bogies.

Nowadays, according to [6], the capability of railway vehicles to efficiently deal with different conditions is gaining in importance, especially in Europe. Indeed, high-speed trains must be able to run also on traditional railroads and, at the same time, standard rail vehicles must be capable of stable high-speed travel. Versatility and interoperability are becoming fundamental features included at the design stage of new railway vehicles.

To overcome the trade-off between the strong damping required during high-speed manoeuvres and the reduced steering resistance advisable when negotiating curves at low speed, several innovative solutions have been studied. In [7], the authors developed and tested (under real conditions) an active electro-mechanical yaw damper to improve the behaviour of the vehicle when travelling along straight and curved tracks. Moreover, in [8], the authors numerically investigated the possibility of reducing the quasistatic guiding force in the outer wheel of the leading wheelset of a

rail vehicle, by introducing active yaw dampers. Further studies have been published on the application of various control logics for Secondary Yaw Control (SYC) strategies to increase vehicle stability and to obtain higher curve-taking performance, also thanks to the simultaneous reduction of yaw stiffness of the bogies [9]. The works discussed proved that a proper SYC strategy may lead to increased vehicle performance when it comes to both high-speed travel and low-speed curve negotiation. Unfortunately, all the solutions mentioned require a specific vehicle design to be implemented and an external power supply to work properly.

In this context, damper manufacturers are working on yaw damper solutions able to properly deal with both high-speed running conditions and low-speed curve negotiation. This paper focuses on an innovative passive yaw damper, the Inverted Frequency Selective Damper (iFSD damper), able to modify its working behaviour according to the vehicle's running conditions. This component was designed by Koni BV to be compatible with various vehicles, due to its capability of replacing standard passive components. Moreover, thanks to its passive nature, this device does not require any kind of external power supply, making it extremely suitable for any kind of railway vehicle. The iFSD yaw damper can decouple the high-frequency behaviour, typical of high-speed running conditions, from the low-frequency behaviour, predominant when negotiating transient small-radius curves, increasing both the high-speed stability and the curve-taking performance of the railway vehicle.

2 Damper characterisation and modelling

2.1 The iFSD yaw damper prototype

The iFSD yaw damper is a smart passive device able to modify its working behaviour according to the railway vehicle's operating conditions. The iFSD damper has been prototyped by introducing two Frequency Selective Damping (FSD) valves, patented by Koni BV, on the piston head of a standard yaw damper. The FSD valves can open a by-pass channel according to the state of a specific reservoir oil chamber. In particular, this by-pass is opened only when the reservoir chamber is completely

empty. The oil flows out from the reservoir chamber according to the relative speed between piston and cylinder and, if the flow direction is maintained for enough time, the chamber can be completely discharged. Therefore, the opening of FSD by-pass occurs when the stroke is monotonic, i.e. constant relative speed sign, for a time interval higher than a designed threshold. Conversely, if the damper speed changes direction, the reservoir chamber is suddenly re-filled, resetting the emptying procedure.

The iFSD smart damper aims at reducing the damper forces through the opening of the by-pass during the negotiation of sharp transient curve segments. Indeed, the stroke of the yaw dampers is defined by two main contributions: a geometric displacement related to the track geometry and a dynamic oscillation caused by track irregularity. During the negotiation of low radius curves, the geometric contribution is much more relevant than the dynamic oscillation. The gradient of the track curvature generates a monotonic stroke of the yaw dampers, causing the complete opening of FSD valves. Since these curves are negotiated at low speed, the reduced damping characteristic does not affect the vehicle dynamics in terms of hunting instability. High and medium speed conditions, instead, are characterized by high curve radii. In these conditions, the geometrical effect becomes less relevant than the dynamic contribution. The continuous oscillation of the piston maintains the reservoir chamber full, prevents the FSD valves opening and keeps the smart damper characteristic equal to that of the standard one. The iFSD technology, based on the autonomous opening of the FSD valves, is applied to standard yaw dampers with the aim of reducing the longitudinal damping forces in transient curve segments, when the low frequency components are predominant on the damper stroke. At the same time, the damping capability of the device is unchanged during high-speed running scenarios, when the stroke frequency spectrum is more related to high frequency contents and where the FSD valves remain closed. The aim of introducing the iFSD technology on yaw dampers is to overcome the typical trade-off between strong damping action, required to assure the stability of the train when running at high-speed, and reduced damping effect, which is advisable for

a limited decrease in curve-taking performance in tight curves.

As a first step of this research, the experimental characterisation procedures for the iFSD and the standard passive yaw dampers were performed on a dedicated test bench. The layout of this test rig is based on the mounting condition of these dampers on a real railway vehicle (figure 1). The test rig design allows typical characterisation procedures to be carried out on yaw dampers positioned at a mounting length of 790 mm and an inclination angle of 6°. The test bench has a servocontrolled MTS® actuator (MTS, Type 248.05, force rating: 50 kN) that imposes the longitudinal displacement on the yaw damper, while a load cell (Hottinger Baldwin Messtechnik, Type U10M/50, adjusted range 50 kN, sensitivity 2.1021 mV/V) measures the actual force provided by the device.

The characterisation procedure is based on the BS EN 13802 standard [10], and it aims to describe the dampers' behaviour by means of hysteresis cycles performed at different combinations of speed, stroke and frequency. Considering that this paper focuses on the behaviour of yaw dampers when negotiating both straight track and tight curves, we considered short and large stroke cycles to emulate a wider range of working conditions. The hydraulic dampers were tested through several of the sinusoidal cycles suggested in Annex F to the EN13802 standard. Moreover, an additional experimental characterization has been performed on both dampers. A set of sinusoidal cycles characterized by the same speed amplitude (30 mm/s) and increasing frequency (from 0.5 to 7 Hz) has been imposed. In this way, it is possible to show the progressive reduction of the FSD by-pass effect. Indeed, as previously described, the iFSD damper requires a monotonic stroke maintained for enough time to open the FSD valves. This condition is not present in short period cycles. For the sake of simplicity and without lack of generality, this paper reports only a reduced selection of such tests, composed of six cycles at constant stroke amplitude and four cycles at constant speed amplitude (figure 1).

The experimental results obtained by the two dampers were compared to highlight the differences introduced by the iFSD technology. Figure 2 presents an overlapping of the hysteresis cycles

measured on both devices: the large stroke tests (figure 2a) are characterised by a strong influence of the FSD valves that can lower the damper forces after a specific amount of time, once the by-pass channel is opened. This allows a sudden reduction in the damper forces transmitted between the car body and the bogies after, for instance, beginning to negotiate a transient curve. The short stroke cycles (figure 2b), on the other hand, can be assumed to be similar to a high-speed running condition. It is interesting to notice that, except for the 10 mm/s test (characterised by a lower frequency), the FSD valves don't affect the damping capability of the device in these conditions. Consequently, the damping force reduction for the iFSD prototype is expected to be present only when negotiating transient curved tracks, without reducing the stabilising effect of the yaw dampers on the vehicle. The comparison between the iFSD and the standard damper cycles at constant speed amplitude (figure 2c) shows that the FSD valves can open only if the monotonic trend of the stroke is maintained for enough time. As expected, the high frequency cycles (2-3 Hz) do not allow to open the by-pass, since the discharging of the reservoir chamber is not completed.

2.2 Numerical modelling of the dampers

In order to properly investigate the vehicle's stability, accurate modelling of the yaw dampers' dynamics is fundamental. According to literature [11], the simplest damper model, based on a linear dashpot, is not sufficient to simulate the component's behaviour. Indeed, the hydraulic shock absorbers are not able to provide a purely damping force, but impose both elastic and damping components. For this reason, the yaw damper's flexibility needs to be considered, and this feature is generally implemented thanks to an in-series stiffness, which composes a typical Maxwell model [12, 13]. The elastic contributions of both damper bushings and internal fluid dynamic phenomena can be modelled. According to [14] and [15], the accuracy of the typical Maxwell model can be further improved by describing the non-linear asymmetric damping ratio of the damper together with asymmetric modelling of its in-series stiffness. These modifications make it possible to correctly simulate the typical asymmetric behaviour of this suspension component.

For this paper, the behaviours of the standard and iFSD yaw dampers were simulated using non-linear models, based on lumped elements and able to calculate the force generated by the component starting from its relative axial stroke. Figure 3 shows a schematic representation of the iFSD damper model, which gives the device force $F_{Damping}$ as output, the imposed displacement x_1 as input. Starting from the aforementioned literature review, the dynamics of the damper were modelled using a 2 degrees of freedom approach by inserting an asymmetric in-series spring to take the component's flexibility into consideration. Moreover, the inertial contribution of the damper mass was considered by introducing a concentrated mass element M between the dashpot and the elastic element. This additional feature is generally neglected due to its low influence on passive devices, whereas when considering the iFSD technology, it plays a fundamental role in cutting the damping force. Another important feature of the model is represented by effects of the FSD valves: an additional by-pass is opened by these valves only when the oil flow direction is maintained for a determined amount of time. The numerical model of the iFSD damper aims to deal with the transition between open and closed FSD valves (and vice-versa) by monitoring the trend of $\dot{x}_2$. When the FSD valves are closed, the iFSD damper behaves like a standard device. The force cutting action, caused by the by-pass opening, is represented by a different force-speed relationship. The comparison between the force-speed functions evaluated during the characterisation experimental tests and related to the FSD valves positions can be observed in figure 4, where the same curve for the passive damper is also reported.

The experimental characterisation was numerically reproduced on the virtual damper models to tune the parameters of the lumped elements and match the experimental hysteresis cycles. The comparison between the experimental and the numerical characterisation cycles is reported in figure 5. The numerical models are able to correctly simulate the dynamics of the two dampers in both large and short stroke cycles. In particular, it is worth noting that the iFSD numerical model is able to properly simulate the force cutting action of the FSD valves in both large and short stroke cycles.

3 Multibody numerical model

In order to validate the performance of the iFSD damper, a railway vehicle equipped with the device was simulated in different operating scenarios - a high-speed straight track and a tight curve negotiated at low speed. A rigid bodies multibody model was designed and implemented in the commercial software, Simpack. The multibody model consists of seven rigid bodies: a car-body, two bogies and four wheelsets. All the simulations were based on a sampling frequency of 1000 Hz. The simulated railway vehicle is equipped with 4 yaw dampers: they were simulated by implementing the in Matlab/Simulink the numerical models presented in section 2. A specific co-simulation routine between Simpack and Matlab/Simulink was set up to correctly estimate the influence of these devices on the vehicle's dynamics. During each simulation time step, the Simpack vehicle model sent the actual displacement to the Matlab/Simulink yaw dampers model, receiving the calculated damper forces as output. Figure 6 shows a panoramic view of the co-simulation procedure including the connection of the Simulink blocks. The Simpack block generates the four signals of the yaw dampers stroke that are sent to the four subsystems representing the damper dynamic models described in section 2. These subsystems calculate and send back to the Simpack block the four damping forces.

The secondary lateral dampers were modelled according to a Maxwell element based on a constant stiffness and a non-linear symmetric dashpot, considering that they play a relevant role in the lateral dynamics of bogies and car-body. Moreover, a non-linear model was implemented for the lateral bumpstops placed within the secondary suspension stage. The secondary vertical dampers and springs were modelled using a linear approach, such as all the suspension components of the primary suspension stage. The dynamic properties of the vehicle are summarised in table 1.

The wheel-rail contact geometry inside the multibody model of the rail vehicle was designed according to a combination widely diffused in Europe. The S1002 wheel profile was modelled according to annex C to the BS EN 13715 standard [16], while modelling of the rail profile was based

on the UIC60 design, choosing a rail cant of 1/40 and a standard gauge of 1435mm. The contact forces between wheels and rails were calculated according to the FASTSIM algorithm [17], considering a friction coefficient equal to 0.4.

As previously introduced, the iFSD yaw damper aims to reduce the ripage forces during low-speed negotiation of tight curves without reducing the vehicle's high-speed stability. For this reason, two specific simulations were designed. The first simulation was based on the annex F to BS EN 14363 [18], the so-called S curve test. It was specifically designed to investigate the behaviour of the railway vehicle while negotiating of switches or crossings. This is an important operating scenario and it was studied, for instance, in [19], given the high influence of switches in the overall maintenance costs of the Swiss national railway network. Also, other studies showed that switches can influence the overall maintenance costs of a railway network by up to 13% [20]. This scenario is characterised by two sudden sharp curves with a radius equal to 190 m, with neither rail superelevation nor rail irregularities implemented. The vehicle's speed was set equal to 43 km/h. The second simulation focused on high-speed running along a straight track where both vertical and alignment rail irregularities were imposed. Starting from the PSD approximation reported in ERRI B176 RPI [21] for German railroads, random spatial histories were generated and imposed along the track. The vehicle speed was set equal to 300 km/h.

4 Numerical results

Numerical simulations were performed by co-simulating the vehicle's multibody model and the two different yaw damper devices described in section 2: the innovative iFSD and the standard version. The same manoeuvres were simulated to compare the two solutions and to quantify their influence on the vehicle's dynamics.

4.1 S curve

The S curve, simulating the negotiation of switches or crossings, produces wide stroke variations of

the vehicle's four yaw dampers. In this condition, the presence of the yaw dampers provides a steering resistance effect on the front and rear bogies and, consequently, it reduces the vehicle's curve-taking performance. In figure 7, the force generated by the four yaw dampers while negotiating a curved track of this kind is shown. It can be observed that the iFSD technology is able to cut the damper force with significant benefits in terms of the vehicle's performance.

The quantification of these performance levels is strongly related to the ripage forces Y (also known as track shifting forces) exchanged between wheelsets and rails. The ripage forces, also known as track shifting forces or guiding forces, are the total lateral force at the wheelset on the rail contact. The lateral direction is defined according to a local right-hand reference system (x,y,z), where x indicates the direction of the rails and z the normal vertical direction. For each wheel-rail pair, the lateral forces are calculated as:

$$Y_L = -F_{z,L} \sin \gamma_L + F_{xy,L} \cos \gamma_L \quad (1)$$

$$Y_R = -F_{z,R} \sin \gamma_R + F_{xy,R} \cos \gamma_R \quad (2)$$

and the ripage force of a single wheelset (front or rear) is expressed as:

$$Y = Y_L + Y_R \quad (3)$$

Indeed, considering an arbitrary wheel (i=L or R, i.e. left or right), γ_i represents the contact angle between the vertical axis z and the normal direction of the wheel-rail contact patch. The guiding forces Y_i are related to the projection of both the vertical load $F_{z,i}$ and the tangential force $F_{xy,i}$. The first contribution is related to the normal load acting on the wheel, while the second term is based on the tangent creep forces generated at the wheel-rail contact patch. $F_{xy,i}$ is computed by Simpack according to the Fastsim algorithm [17]:

$$F_{xy,i} = F_{x,i} + F_{y,i} + M_{z,i} \quad (4)$$

In our analysis, we compared Y for each wheelset in terms of peak of absolute value and RMS value.

The Y force is calculated for each wheelset as the sum of the contact forces imposed by the two wheels on the rails in lateral direction; according to BS EN 14363, this force is low pass filtered

with a cut-off frequency of 20 Hz. Figure 8 compares the trends of the front bogie wheelsets for both the standard and the iFSD solutions. The reduction of Y on the leading wheelset (the most critical) induces a strong improvement in the safety margin calculated according to the BS EN 14363 threshold. A similar trend can be observed for the rear bogie as well, however, it presents lower values of contact forces and is therefore not reported.

Starting from this data, the safety index is quantified according to the Y/Q ratio, which describes the tendency of the vehicle's wheels to show "flange climbing" phenomena (one of the most typical causes of derailment). For an i-esimal wheel, the $(Y/Q)_i$ index is defined as the absolute value of the ratio between the guiding force Y_i and the vertical reaction force Q_i:

$$(Y/Q)_L = \left|\frac{Y_L}{Q_L}\right| = \left|\frac{-F_{z,L}\sin\gamma_L + F_{xy,L}\cos\gamma_L}{F_{z,L}\cos\gamma_L + F_{xy,L}\sin\gamma_L}\right| \quad (5)$$

$$(Y/Q)_R = \left|\frac{Y_R}{Q_R}\right| = \left|\frac{-F_{z,R}\sin\gamma_R + F_{xy,R}\cos\gamma_R}{F_{z,R}\cos\gamma_R + F_{xy,R}\sin\gamma_R}\right| \quad (6)$$

In our analysis, we compared the Y/Q for each wheel of the front bogie in terms of peak value.

According to the BS EN 14363 standard, the general safety threshold of Y/Q is 0.8. Nevertheless, it is recognised that higher values may be encountered during transition curves, such as the S curve manoeuvre. In these conditions, a maximum limit of 1.2 is allowed. The safety enhancement obtained with the adoption of the iFSD yaw dampers can be observed in figure 9, which reports a comparison of the Y/Q trends for the four wheels of the front bogie during negotiation of the S-curve manoeuvre. It can be noticed that the iFSD dampers tend to reduce the Y/Q trends in the most stressed conditions, leading to an overall increase in the operational safety of the vehicle. The Y/Q ratios were low pass filtered with a cut-off frequency of 20 Hz.

It is worth of considering that poor curve-taking performance is strictly related to the generation of relevant wear phenomena at the wheel-rail interfaces. To quantify their effect, it is possible to introduce the Wear Number (WN). The Wear Number of an i-esimal wheel is defined starting from the tangential force $F_{xy,i}$. Thus, WN_i is calculated as:

$$WN_i = \left|F_{x,i}\varepsilon_x\right| + \left|F_{y,i}\varepsilon_y\right| + \left|M_{z,i}\varphi_z\right| \quad (7)$$

where ε_x is the longitudinal, ε_y the lateral and φ_z the spin creepage. In our analysis, we compared the Wear Number indexes in terms of RMS value.

This parameter has already been used as a starting physical index for the optimization of switches layouts [22]. The WN was low pass filtered with a cut-off frequency of 20 Hz. In figure 10, we compare the WN of the front bogie wheels between the two vehicle configurations. The iFSD is able to increase the performance of the leading wheels, which is the most severe case, with minor worsening in the two trailing wheels.

4.2 Straight track manoeuvre

This high-speed manoeuvre was studied to verify the stability of the vehicle. Indeed, the iFSD damper proved to be a valid solution for reducing lateral force in small-radius curves, but this advantage must be achieved without decreasing its stabilising effect when the vehicle is travelling at high-speed.

Again, based on the EN 14363 standard, quantification of the vehicle's stability during this manoeuvre was obtained by comparing a specific performance index, obtained from the bogie's lateral acceleration measured over the axle box, according to the following procedure:

- The reference frequency f0 is defined from a high-speed running of the test case vehicle without damping. It is defined as the dominant frequency identified in the unstable motion of the vehicle.
- A band-pass filter, centred on the f0 frequency, is applied to the bogie's lateral acceleration measured over the axle box ($\ddot{y}_b$). The bandpass window width is ±2 Hz.
- The filtered bogie lateral acceleration ($\ddot{y}_{b,filt}$) is processed according to a sliding Root Mean Squared (RMS) value, considering a window length L_W of 100 m and a minimum overlap factor of 0.9. As an example, the $\ddot{y}_{b,filt,RMS}$ acceleration related to the first window is:

$$\ddot{y}_{b,filt,RMS} = \frac{1}{N}\sqrt{\sum_{1}^{N} \ddot{y}_{b,filt}} \quad (8)$$

The number of samples N is related to the vehicle speed (v) and the time step (t_{Step}) of the multibody simulation:

$$N = \frac{L_W}{v\, t_{Step}} \quad (9)$$

In our analysis, we compared the peak value of $\ddot{y}_{b,filt,RMS}$.

In figure 11, the comparison between the processed accelerations with standard and iFSD dampers is shown for both the front and rear bogie. We can observe that in a typical high-speed operating scenario, the iFSD damper is able to maintain its stabilizing effect by limiting the bogies' lateral accelerations of the vehicle. According to EN 14363, the stability threshold for RMS lateral acceleration is 5.77 m/s^2 for the vehicle simulated; the highest RMS value obtained during the simulation must respect this limit. The iFSD damper provides a percentage variation of the RMS maximum value equal to -0.88% for the front bogie (from 0.351 m/s^2 of the standard solution to 0.348 m/s^2) and -7.42% for the rear bogie (from 0.384 m/s^2 of the standard solution to 0.356 m/s^2). This comparison proves that the innovative damper is able to increase the train's curve-taking performance without reducing its standard stability performance. For the sake of simplicity, the presented results refer to two limit cases (tangent track and switch negotiation). Appendix A reports a comprehensive summary of the vehicle performances with standard and iFSD dampers in these limit conditions. To verify the performances also in intermediate conditions, an extended analysis has been performed considering different scenarios (curve radius from 400 to 1200 m), which show the progressive reduction of the FSD by-pass effect for wider curves (appendix B).

4.3 The modified iFSD damper

However, in order to numerically investigate the full potential of the iFSD solution, we set up an

additional damper numerical model (iFSD MOD) simulating an iFSD with a stronger damping capability in a closed valve condition. The force-speed characteristic curve is reported in figure 12. Following the same approach as in the previous sections, the new iFSD model was tested to verify the possibility of achieving higher stability performance during high-speed running together with better curve-taking performance while negotiating small-radius curves. The comparison of the bogie's lateral accelerations between a rail vehicle with passive and iFSD MOD dampers is shown in figure 13. The iFSD MOD damper improves the vehicle stability with a percentage variation of the RMS maximum value equal to -13.5% for the front bogie (corresponding to 0.304 m/s^2) and -15.4% for the rear bogie (corresponding to 0.325 m/s^2).

As a last step we also verified the iFSD MOD performance during low-speed negotiation of the small-radius S curve. Figure 14 reports a comparison of the front bogie's ripage forces, which is the most important performance index in terms of curve-taking performance, for the dampers considered. The iFSD MOD shows a behaviour very similar to that of the iFSD, characterized by a strong reduction in the ripage forces compared to the standard yaw damper. These results confirm the possibility of overcoming the typical trade-off between high-speed running and low-speed curve negotiation by using iFSD technology. Appendix A summarizes the vehicle performances with iFSD MOD damper in the two limit conditions (tangent track and switch negotiation).

5 Conclusions

In this work, the innovative iFSD yaw damper was studied. This device aims to increase the curve-taking performance of high-speed railway vehicles without reducing their high-speed stability. An experimental characterisation campaign was performed on an iFSD prototype, together with a standard passive component, to highlight the differences between their characteristic curves and to show the capability of the innovative damper to adapt its behaviour to different conditions. Two different non-linear models were designed to simulate the dampers' dynamics and to be implemented inside a multibody model of a railway vehicle. An innovative approach was introduced to simulate

the behaviour of the iFSD damper during its two different working phases. Moreover, the models were designed and tuned to match the experimental data obtained from the characterisation campaign.

The vehicle's performance obtained with the iFSD damper was compared to the standard damper performance in two different operative scenarios: a small-radius S curve, negotiated at low speed, and a straight track segment, simulated at high speed. In the small-radius curves, the iFSD dampers proved to significantly reduce the ripage forces of the different wheelsets (with an absolute reduction greater than 10 kN and a percentage reduction of about 35%). Moreover, implementation of iFSD damper showed a reduction of both Y/Q and wear number performance indexes, indicating an increased safety level and a reduction of the wear phenomena. The straight track simulation showed that the innovative damper does not reduce the vehicle's stability performance indexes while travelling at high-speed.

Finally, a numerical simulation of a modified version of the innovative damper (the iFSD MOD), characterised by a stronger damping action in the closed valve condition, was developed. This analysis illustrated the possibility to further develop this technology, increasing the maximum force that the smart yaw damper can generate in high-speed running conditions. This new model proved to enhance the vehicle's stability, with a reduction in the lateral acceleration for both the front and the rear bogie, maintaining the same iFSD improvement as obtained in curves.

In conclusion, the iFSD yaw damper proved to be a valid alternative to the standard passive yaw damper. The intrinsic passive nature of this device and its adaptable mounting length, make this solution particularly interesting for use on both new and existing vehicles, with the final aim of increasing their interoperability, safety and competitiveness.

Declaration of interest statement

No potential conflict of interest was reported by authors.

1 **References**

2

[1] M. Givoni, C. Brand and P. Watkiss, "Are Railways 'climate friendly'?," *Built Environment,* vol. 35, pp. 70-86, 2009.

[2] F. Dobruszkes, "High-speed rail and air transport competition in Western Europe: A supply-oriented perspective," *Transport Policy,* vol. 18, no. 6, pp. 870-879, 2011.

[3] B. Fu, R. L. Giossi, R. Persson, S. Stichel, S. Bruni and R. Goodall, "Active suspension in railway vehicles: a literature survey," *Railway Engineering Science,* vol. 28, no. 1, pp. 3-35, 2020.

[4] A. Alonso, J. G. Gimenez and E. Gomez, "Yaw damper modelling and its influence on railway dynamic stability," *Vehicle System Dynamics,* vol. 49, no. 9, pp. 1367-1387, 2011.

[5] Z. Xia, J. Zhou, D. Gong, W. Sun and Y. Sun, "Theoretical study on the effect of the anti-yaw damper for rail vehicles," *Proceedings of the Insitution of Mechanical Engineers, Part C: Journal of Mechanical Engineering Science,* vol. 23, pp. 457-473, 2019.

[6] J. Campos and G. de Rus, "Some stylized facts about high-speed rail: A review of HSR experiences around the world," *Transport Policy,* vol. 16, no. 1, pp. 19-28, 2009.

[7] F. Braghin, S. Bruni and F. Resta, "Active Yaw Damper for the Improvement of Railway Vehicle Stability and Curving Performances: Simulations and Experimental Results," *Vehicle System Dynamics,* vol. 44, no. 11, pp. 857-869, 2006.

[8] T. Michalek and J. Zelenka, "Reduction of Lateral Forces Between the Railway Vehicle and the Track in Small-Radius Curves by means of Active Elements," *Applied and Computational Mechanics,* vol. 5, 12 2011.

[9] S. Alfi, D. Prandi, C. P. Ward, S. Bruni and R. M. Goodall, "Active Secondary Yaw Control to Improve Curving Behaviour of a Railway Vehicle," *The Proceedings of International*

Symposium on Seed-up and Service Technology for Railway and Maglev Systems : STECH, 2015.

[10] BSI Standards Publication, *BS EN 13802 Railway applications — Suspension components — Hydraulic dampers*, 2013.

[11] S. Bruni, J. Vinolas, M. Berg, O. Polach and S. Stichel, "Modelling of suspension components in a rail vehicle dynamics context," *Vehicle System Dynamics*, pp. 1021-1072, 2011.

[12] M. Wrang, "Instability Phenomena of a Passenger Coach, Caused by Internal Yaw Damper Flexibility," *Vehicle System Dynamics*, vol. 33, no. Supplement 1, pp. 406-417, 1999.

[13] S. Bruni, P. Belforte, H. Hartwig, G. Mancini and L. Mazzola, "Experimental investigation of yaw damper performances: an improved and harmonised testing," in *WCRR'08 international conference*, Seoul, 2008.

[14] A. C. Mellado, J. Vinolas and E. Gomez, "Advances on railway yaw damper characterization exposed to small displacements," *International journal of heavy vehicle systems IJHVS*, vol. 13, 2006.

[15] W. Teng, H. Shi, R. Luo, J. Zeng and C. Huang, "Improved nonlinear model of a yaw damper for simulating the dynamics of a high-speed train," *Proceedings of the Institution of Mechanical Engineers Part F Journal of Rail and Rapid Transit*, vol. 233, no. 7, pp. 651-665, 2018.

[16] BSI Standards Publication, "BS EN 13715 Railway applications — Wheelsets and bogies — Wheels — Tread Profile," 2020.

[17] J. J. Kalker, "A Fast Algorithm for the Simplified Theory of Rolling Contact," *Vehicle System Dynamics*, vol. 11, no. 1, pp. 1-13, 1982.

[18] BSI Standards Publication, "BS EN 14363 Railway applications - Testing ans Simulation for the acceptance of running characteristics of railway vehicles - Running Behaviour and stationary tests".

[19] T. Michalek and M. Kohout, "On the problems of lateral force effects of railway vehicles in S-curves," *Vehicle System Dynamics,* vol. 0, no. 0, pp. 1-19, 2021.

[20] A. Nissen, "Classification and cost analysis of switches and crossings for the Swedish railway: a case study," *Journal of Quality in Maintenance Engineering,* vol. 15, pp. 202-220, 2009.

[21] *ERRI B176 RPI Bogies with steered or steering wheelsets,* Utrecht.

[22] B. A. Palsson, "Design optimisation of switch rails in railway turnouts," *Vehicle System Dynamics,* vol. 51, no. 10, pp. 1619-1639, 2013.

[23] BSI Standards Publication, *BS EN 14363 Railway applications - Testing and Simulation for the acceptance of running characteristics of railway Running Behaviour and stationary tests,* 2018.

A Appendix

Curving performances			
	Standard damper	iFSD damper	iFSD MOD damper
Peak value of $Y_{Front\ Wheelset}$	72500 N	53053 N	53200 N
Peak value of $Y_{Rear\ Wheelset}$	35601 N	24299 N	29827 N
RMS value of $Y_{Front\ Wheelset}$	20251 N	13045 N	13293 N
RMS value of $Y_{Rear\ Wheelset}$	13916 N	6997 N	7565 N
Peak value of $\frac{Y}{Q_{FL}}$	0.958	0.838	0.844
Peak value of $\frac{Y}{Q_{FR}}$	0.776	0.696	0.708
Peak value of $\frac{Y}{Q_{RL}}$	0.509	0.326	0.355
Peak value of $\frac{Y}{Q_{RR}}$	0.530	0.298	0.309
RMS value of WN_{FL}	366.70 N	300.82 N	311.75 N
RMS value of WN_{FR}	365.10 N	302.52 N	317.29 N
RMS value of WN_{RL}	168.87 N	164.14 N	169.88 N
RMS value of WN_{RR}	157.93 N	140.13 N	146.25 N
Stability performances			
	Standard damper	iFSD damper	iFSD MOD damper
Max $\ddot{y}_{b,filt,RMS}$ front bogie	0.351 m/s^2	0.348 m/s^2	0.304 m/s^2
Max $\ddot{y}_{b,filt,RMS}$ rear bogie	0.384 m/s^2	0.356 m/s^2	0.325 m/s^2

B Appendix

Track features				Curve entry transient		Curve constant radius		Curve exit transient	
	Radius [m]	Cant [m]	Vehicle Speed [km/h]	$Y_{RMS,Front}$ Standard damper [N]	$Y_{RMS,Front}$ iFSD damper [N]	$Y_{RMS,Front}$ Standard damper [N]	$Y_{RMS,Front}$ iFSD damper [N]	$Y_{RMS,Front}$ Standard damper [N]	$Y_{RMS,Front}$ iFSD damper [N]
Curve 1	400	0.115	90	15615	8694	1692	1560	11414	8375
				Variation: -44.3%		Variation: -7.8%		Variation: -26.6%	
Curve 2	600	0.115	110	8267	6797	8555	8166	8549	7256
				Variation: -17.8%		Variation: -4.6%		Variation: -15.1%	
Curve 3	800	0.127	130	4497	4481	3920	3815	7604	7122
				Variation: -0.3%		Variation: -2.7%		Variation: -6.3%	
Curve 4	1000	0.12	150	3656	3712	3104	3085	5012	4875
				Variation: 1.8 %		Variation: -0.6 %		Variation: -2.7 %	
Curve 5	1200	0.16	170	3538	3537	4067	4048	4922	4871
				Variation: 0.0 %		Variation: -0.5 %		Variation: -1.0 %	

Tables

Primary longitudinal stiffness	$k_{x,I}$	5.516 E07 N/m
Primary lateral stiffness	$k_{y,I}$	1.316 E07 N/m
Primary vertical stiffness	$k_{z,I}$	9.700 E05 N/m
Primary longitudinal damping	$r_{x,I}$	5.500 E04 Ns/m
Primary lateral damping	$r_{y,I}$	1.500 E04 Ns/m
Primary vertical damping	$r_{z,I}$	3.200 E04 Ns/m
Secondary longitudinal stiffness	$k_{x,II}$	1.450 E05 N/m
Secondary lateral stiffness (spring)	$k_{y,II}$	1.450 E05 N/m
Secondary lateral bumpstops		Non-linear model
Secondary vertical stiffness	$k_{z,II}$	3.410 E05 N/m
Anti-roll bar stiffness	$k_{\theta,II}$	6.239 E06 N/rad
Secondary longitudinal damping (yaw dampers)		Matlab/Simulink model
Secondary lateral damping		Non-linear model
Secondary vertical damping	$r_{z,II}$	3.0 E04 Ns/m
Wheelset mass	m_w	1873 kg
Wheelset moment of inertia, x	$I_{xx,w}$	1260 kgm^2
Wheelset moment of inertia, y	$I_{yy,w}$	125 kgm^2
Wheelset moment of inertia, z	$I_{zz,w}$	1260 kgm^2
Bogie mass	m_b	2775 kg
Bogie moment of inertia, x	$I_{xx,b}$	2015 kgm^2
Bogie moment of inertia, y	$I_{yy,b}$	1664 kgm^2

Bogie moment of inertia, z	$I_{zz,b}$	3479 kgm^2
Car-body mass	m_c	3.645 E04 kg
Car-body moment of inertia, x	$I_{xx,c}$	5.973 E04 kgm^2
Car-body moment of inertia, y	$I_{yy,c}$	1.712 E06 kgm^2
Car-body moment of inertia, z	$I_{zz,c}$	1.712 E06 kgm^2

1 Table 1 Dynamic properties of the multibody model.

2

3 **Figures**

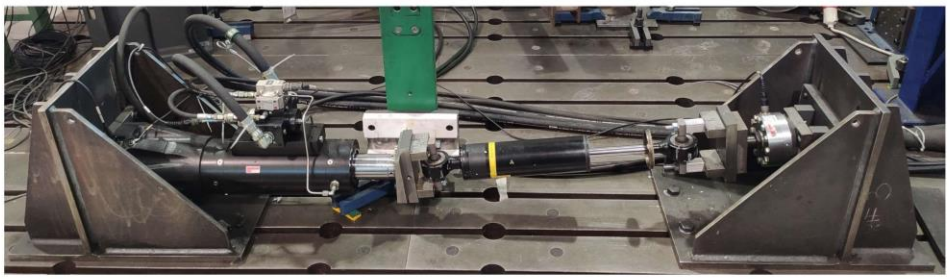

Constant stroke cycles				
	Short stroke cycles		Large stroke cycles	
Speed [mm/s]	Frequency [Hz]	Stroke [mm]	Frequency [Hz]	Stroke [mm]
10	0.637	2.5	0.064	25
30	1.91	2.5	0.191	25
100	6.37	2.5	0.637	25

Constant speed cycles		
Frequency [Hz]	Speed [mm/s]	Stroke [mm]
0.5	30	9.55
1	30	4.78
2	30	2.39
3	30	1.59

4

5 Figure 1

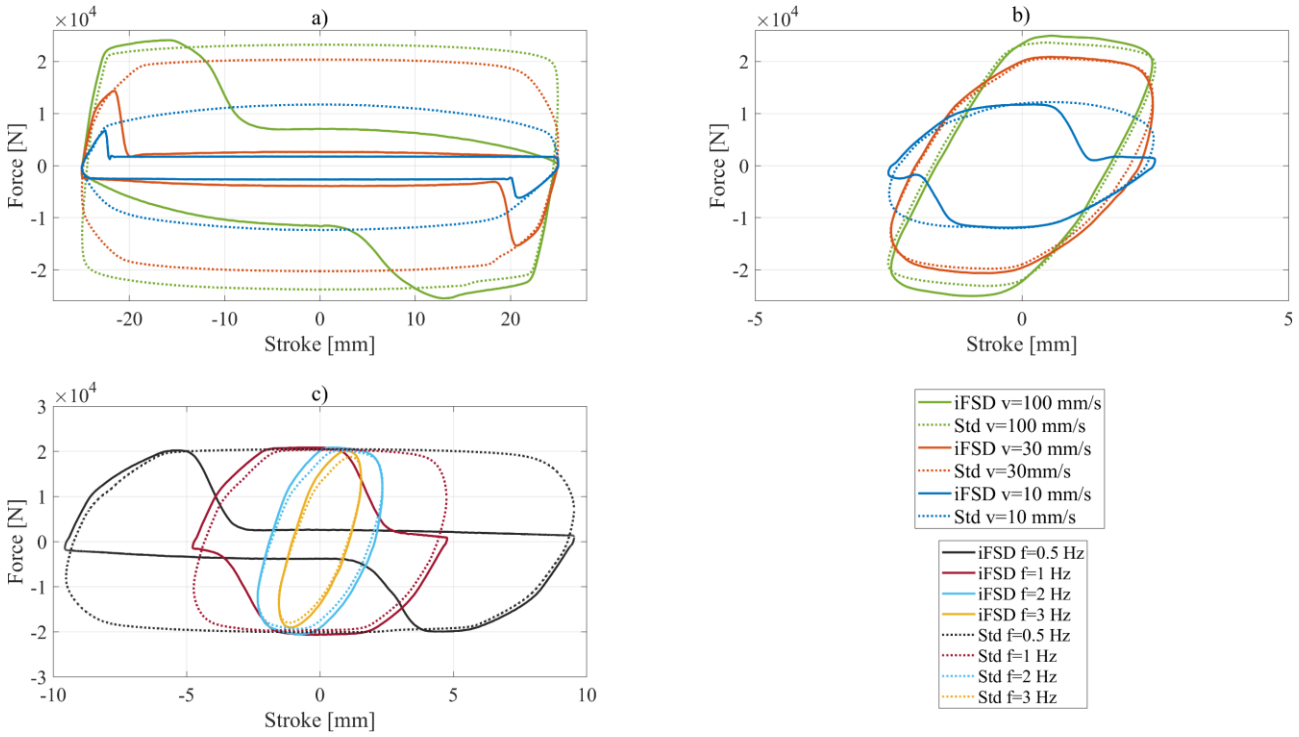

Figure 2

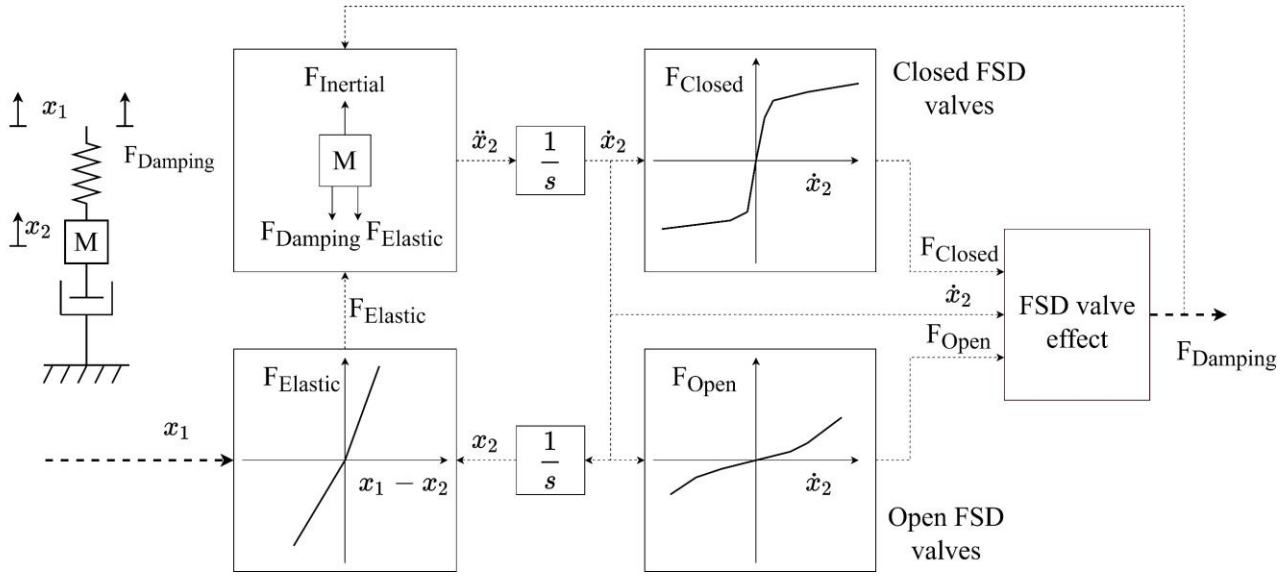

Figure 3

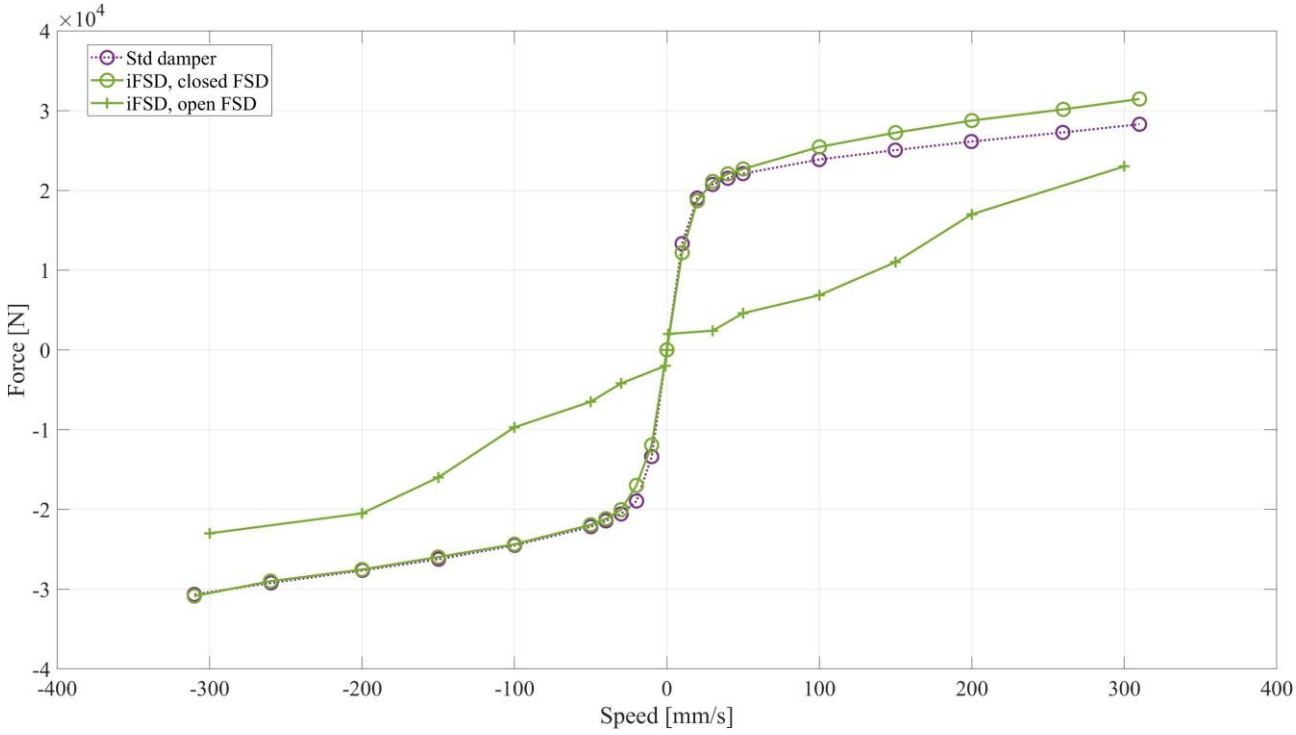

Figure 4

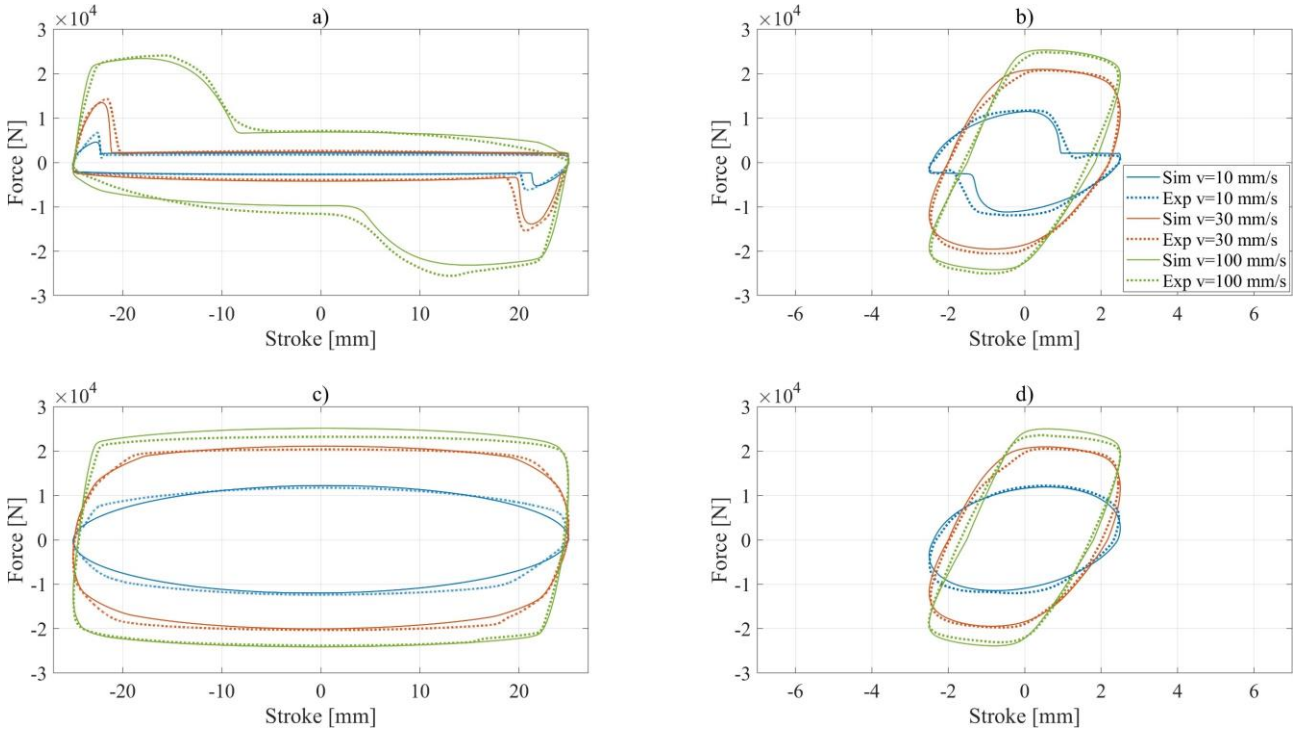

Figure 5

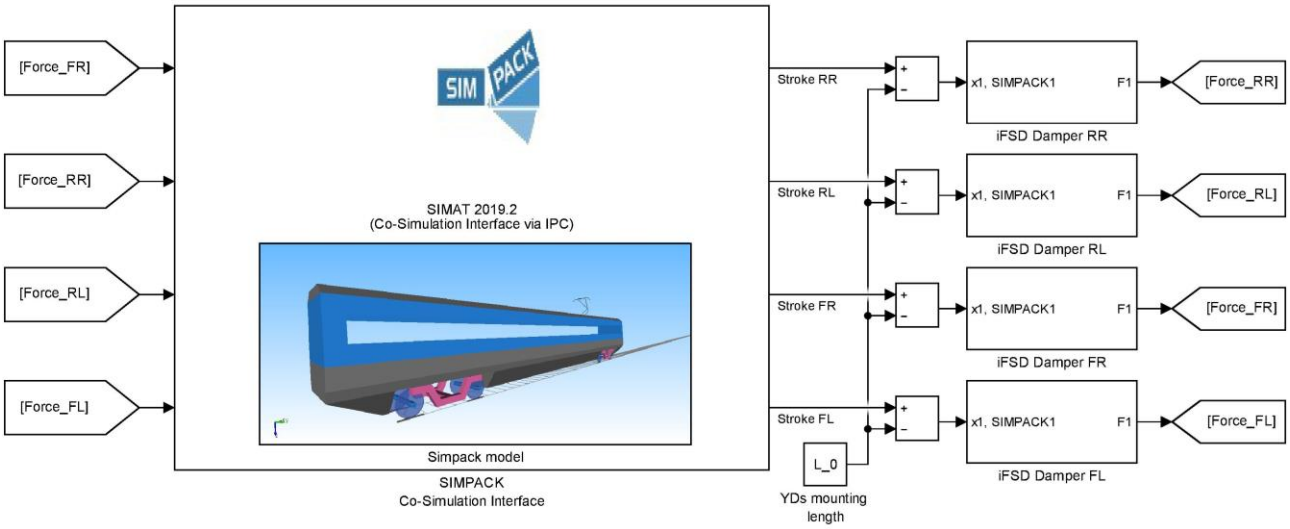

1

2 Figure 6

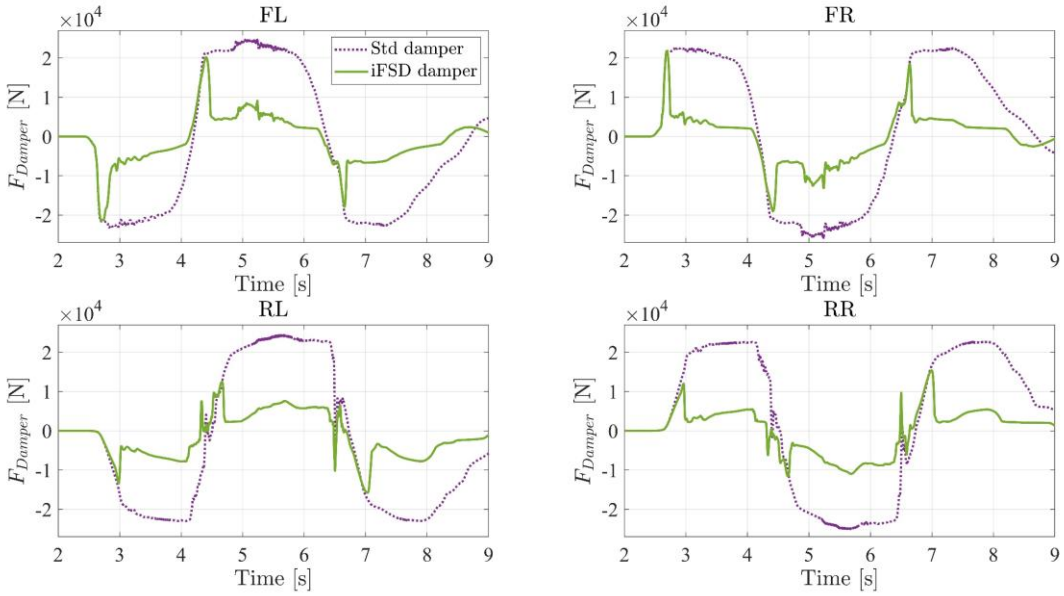

3

4 Figure 7

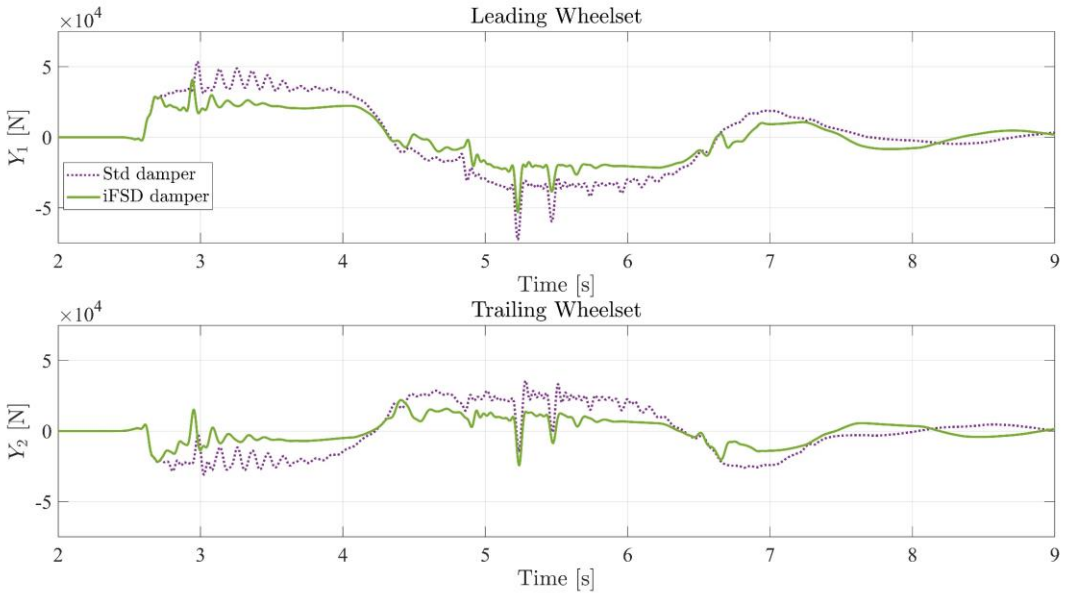

1

2 Figure 8

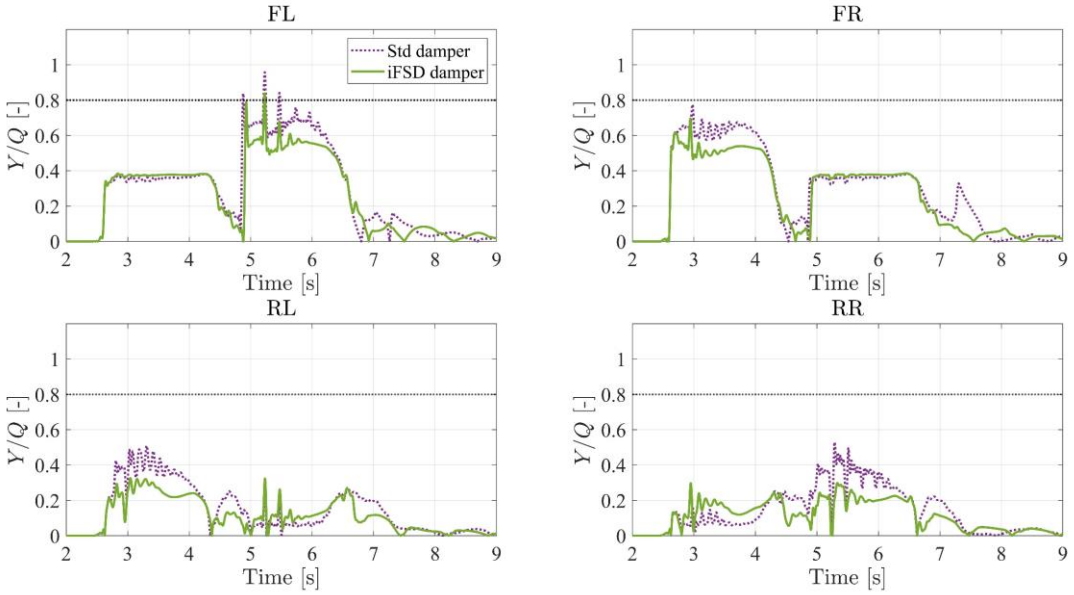

3

4 Figure 9

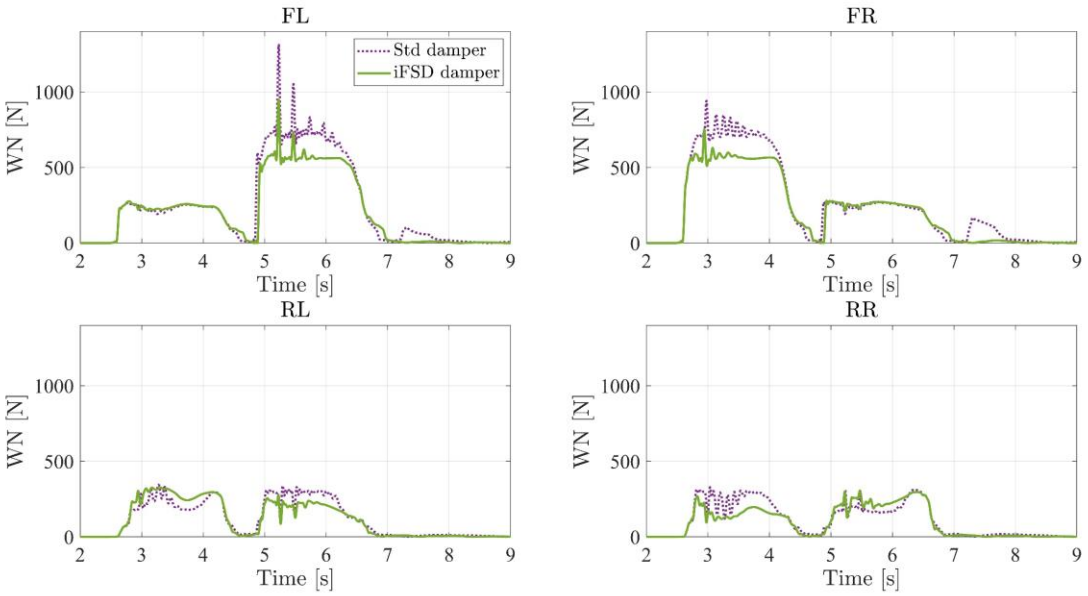

Figure 10

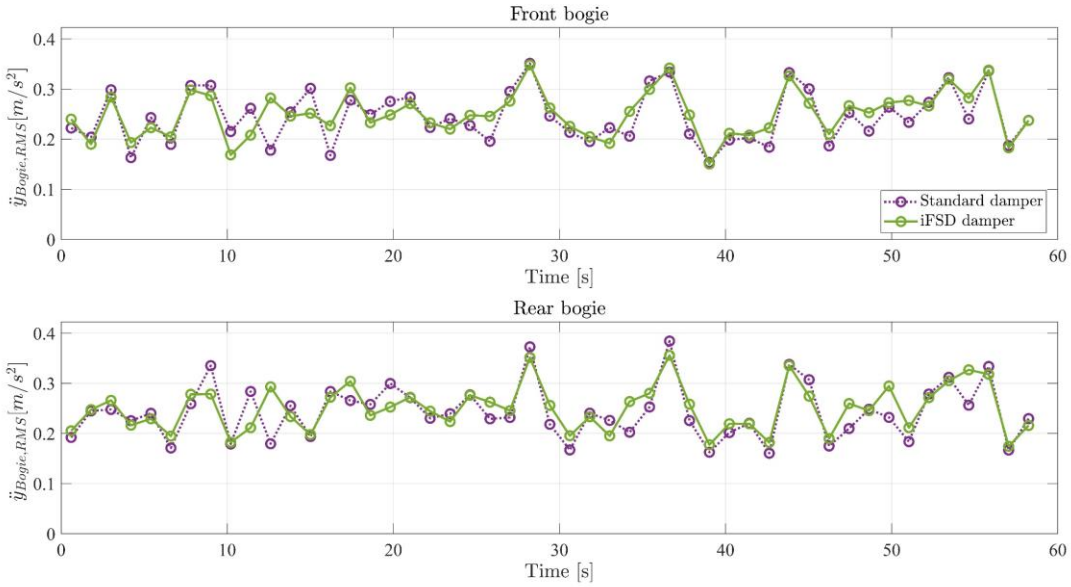

Figure 11

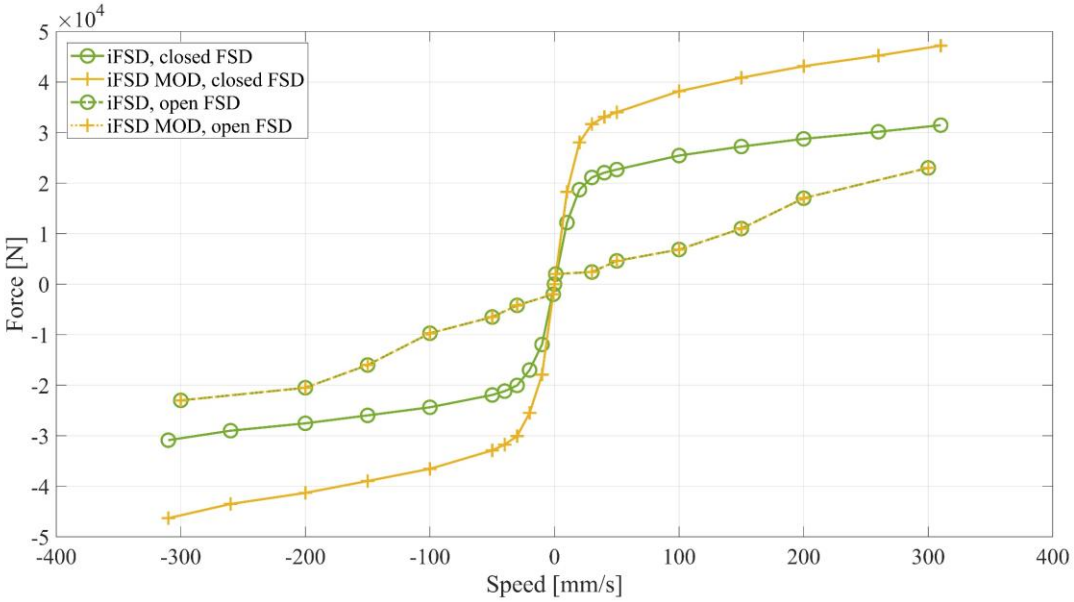

1

2 Figure 12

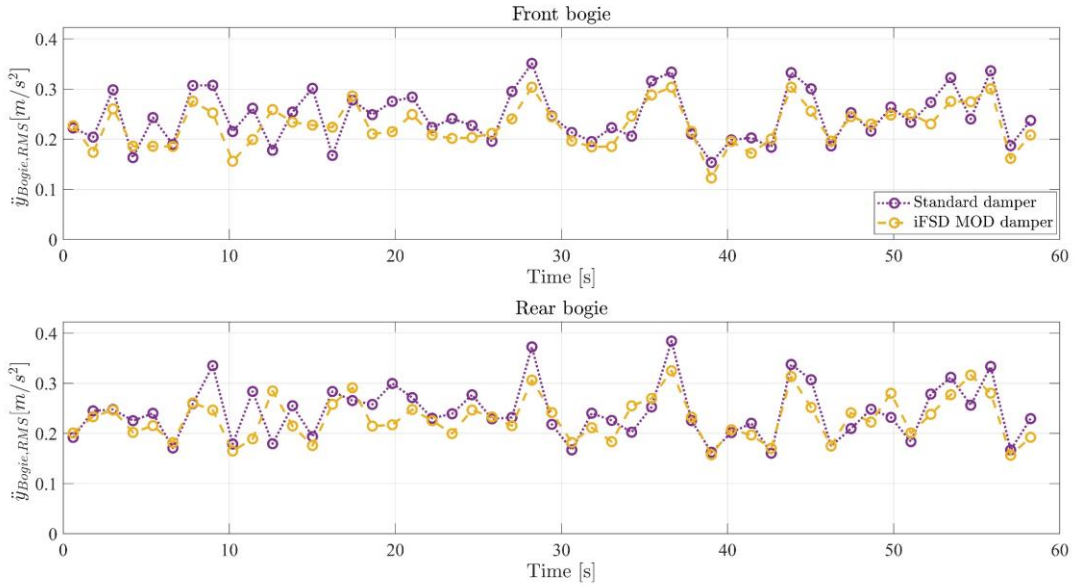

3

4 Figure 13

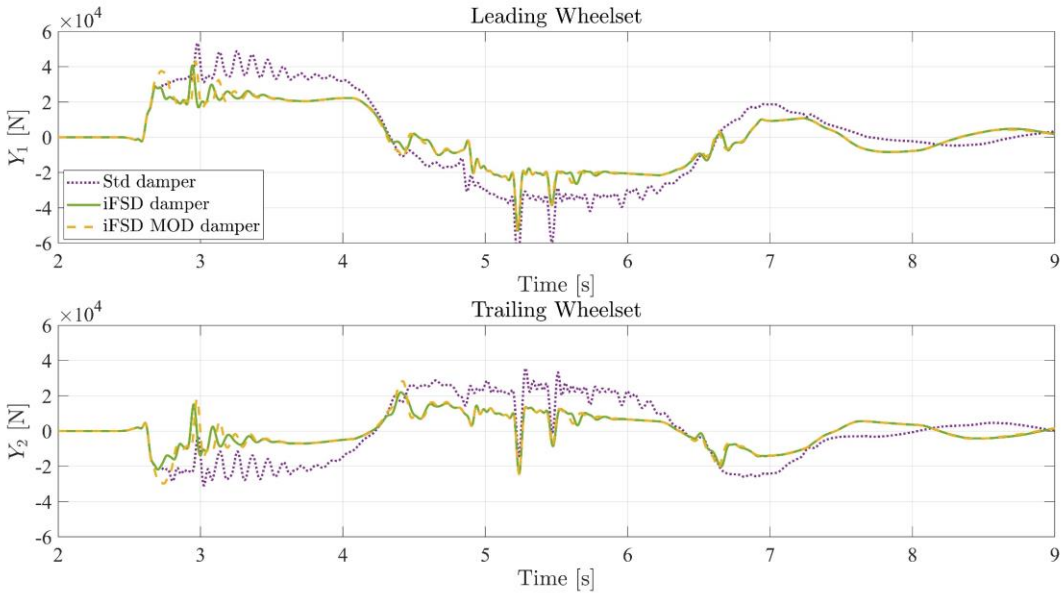

Figure 14

Figure captions

Figure 1: Experimental test bench for yaw damper characterisation. Summary of relevant sinusoidal cycles.

Figure 2 Hysteresis cycles obtained during the experimental characterisation procedure applied to both iFSD and standard dampers. Comparison between results obtained during large stroke tests (a), short stroke tests (b), constant speed tests (c).

Figure 3 Schematic representation of the non-linear model of the iFSD damper: block concept based on the 2 dof model.

Figure 4 Comparison of the force-speed relationships of the Standard damper and the iFSD damper working under the two different conditions of the FSD valves.

Figure 5 Comparison between damper force measured during the experimental characterisation cycles (Exp) and the numerical force simulated using the Simulink model (Sim); large stroke tests on iFSD (a), short stroke tests on iFSD (b), large stroke tests on standard damper (c), short stroke tests on standard damper (d).

Figure 6 Panoramic representation of the co-simulation procedure between the Simpack vehicle model and the Matlab/Simulink damper models.

Figure 7 S curve simulation: comparison between the yaw damper forces performed during multibody simulation using a standard damper and an iFSD damper. FL: Front Left yaw damper, FR: Front Right yaw damper, RL: Rear Left yaw damper, RR: Rear Right yaw damper.

Figure 8 S curve simulation: comparison between the ripage forces of the two wheelsets of the front bogie during multibody simulations with iFSD or Standard dampers.

Figure 9 S curve simulation: comparison between the Y/Q ratio of the front bogie wheels during multibody simulations with iFSD or Standard dampers. iFSD damper: comparison of the Y/Q derailment index. FL: Front Left wheel, FR: Front Right wheel, RL: Rear Left wheel, RR: Rear Right wheel.

Figure 10 S curve simulation: comparison between the Wear Numbers of the front bogie wheels during the multibody simulations with iFSD or Standard dampers. iFSD damper. FL: Front Left wheel, FR: Front Right wheel, RL: Rear Left wheel, RR: Rear Right wheel.

Figure 11 Straight track simulation: comparison between the RMS lateral acceleration of the bogies during the multibody simulations with iFSD or Standard dampers iFSD damper.

Figure 12 Comparison of force-speed relationships between the iFSD and iFSD MOD dampers working under the two different FSD valve conditions.

Figure 13 Straight track simulation: comparison between the RMS lateral acceleration of the bogies during the multibody simulations with iFSD MOD or Standard dampers.

Figure 24 S curve simulation: comparison between the ripage forces of the two wheelsets of the front bogie during the multibody simulations with iFSD, iFSD MOD and Standard dampers.